Cell Reports

Resource

Hair Follicle Development in Mouse Pluripotent Stem Cell-Derived Skin Organoids

Graphical Abstract

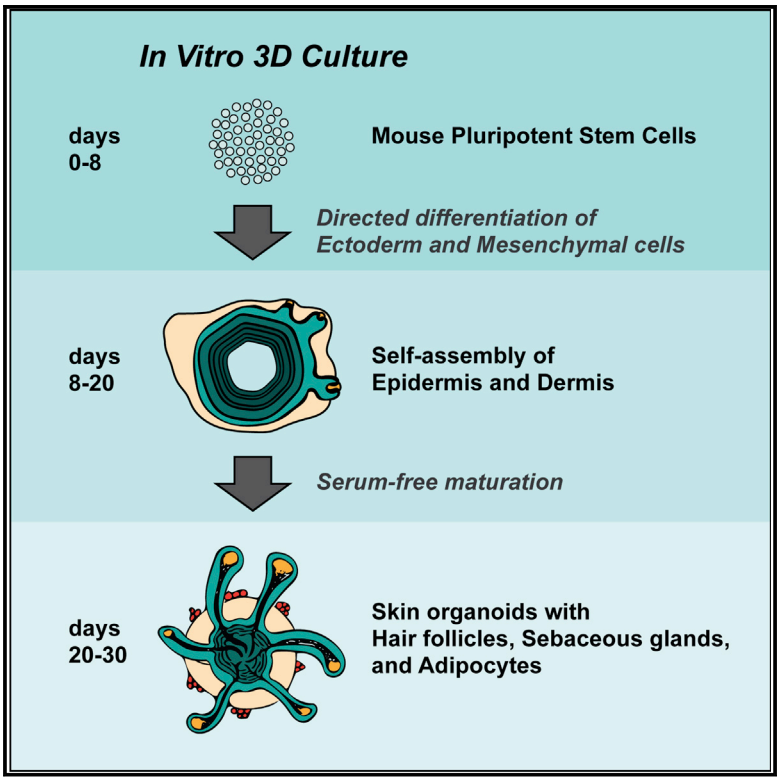

Highlights

- Skin organoids can be generated from mPSCs under defined conditions
- Skin organoids are composed of self-assembled epidermal and dermal layers
- Skin organoids produce hair follicles, sebaceous glands, and adipocytes
- Hair follicle induction from skin organoids mimics normal hair folliculogenesis

Authors

Jiyoon Lee, Robert Böscke, Pei-Ciao Tang, Byron H. Hartman, Stefan Heller, Karl R. Koehler

Correspondence

krkoehle@iu.edu

In Brief

Lee at el. describe a defined *in vitro* 3D culture system that generates skin organoids from mouse pluripotent stem cells. The skin organoids contain self-organized skin layers and skin appendages, including hair follicles, sebaceous glands, and adipocytes.

Lee et al., 2018, Cell Reports *22*, 242–254
January 2, 2018
https://doi.org/10.1016/j.celrep.2017.12.007

CellPress

OPEN ACCESS
CellPress

Cell Reports
Resource

Hair Follicle Development in Mouse Pluripotent Stem Cell-Derived Skin Organoids

Jiyoon Lee,[1] Robert Böscke,[2] Pei-Ciao Tang,[1] Byron H. Hartman,[2] Stefan Heller,[2] and Karl R. Koehler[1,3,*]
[1]Department of Otolaryngology-Head and Neck Surgery, Indiana University School of Medicine, Indianapolis, IN 46202, USA
[2]Department of Otolaryngology-Head and Neck Surgery, Stanford University School of Medicine, Stanford, CA 94305, USA
[3]Lead Contact
*Correspondence: krkoehle@iu.edu
https://doi.org/10.1016/j.celrep.2017.12.007

SUMMARY

The mammalian hair follicle arises during embryonic development from coordinated interactions between the epidermis and dermis. It is currently unclear how to recapitulate hair follicle induction in pluripotent stem cell cultures for use in basic research studies or *in vitro* drug testing. To date, generation of hair follicles *in vitro* has only been possible using primary cells isolated from embryonic skin, cultured alone or in a co-culture with stem cell-derived cells, combined with *in vivo* transplantation. Here, we describe the derivation of skin organoids, constituting epidermal and dermal layers, from a homogeneous population of mouse pluripotent stem cells in a 3D culture. We show that skin organoids spontaneously produce *de novo* hair follicles in a process that mimics normal embryonic hair folliculogenesis. This *in vitro* model of skin development will be useful for studying mechanisms of hair follicle induction, evaluating hair growth or inhibitory drugs, and modeling skin diseases.

INTRODUCTION

The integumentary system consists of skin and its appendages. The skin is composed of two layers, the epidermis and the dermis, which produce appendages, such as hair follicles (HFs), sweat glands, and nails. While the epidermis of the skin arises from the ectoderm, the dermis has different embryonic origins. The majority of the body dermal tissue arises from paraxial and lateral plate mesoderm, while facial dermis arises from cranial neural crest cells (Dequéant and Pourquié, 2008; Driskell and Watt, 2015; Fernandes et al., 2004). Regardless of dermal origin, all skin types require the interplay of epithelial (epidermis) and mesenchymal (dermis) cells for terminal development and appendage formation. In animal models, rodent and human skin with HFs can be reconstituted by co-culturing mesenchymal cells with epithelial cells or, specifically, HF-initiating dermal papilla (DP) cells (Asakawa et al., 2012; Chuong et al., 2007; Ehama et al., 2007; Ikeda et al., 2009; Nakao et al., 2007; Takagi et al., 2016; Toyoshima et al., 2012; Zheng et al., 2005). However, a chemically defined means of generating folliculogenic skin from pluripotent stem cells (PSCs) *in vitro* has been intangible.

To date, *in vitro* skin derivation strategies have focused on generating keratinocytes and fibroblasts from PSCs in separate cultures first and then combining the two types of cells to form a skin-like bilayer (Gledhill et al., 2015; Itoh et al., 2013; Oh et al., 2013; Sun et al., 2014). Recently, we developed a three-dimensional (3D) mouse embryonic stem cell (mESC) culture capable of producing cranial surface epithelia (also known as non-neural ectoderm), a precursor tissue of the skin epidermis. In the process of culture, a heterogeneous population of mesenchymal and neural cells is also generated (Koehler and Hashino, 2014; Koehler et al., 2013). Using this technique, we have demonstrated how to generate inner ear organoids that contain sensory epithelia reminiscent of postnatal mouse vestibular organs (Koehler et al., 2013; Koehler and Hashino, 2014). In addition, we also briefly described how the induced surface epithelia generate $p63^+$ keratin 5 $(KRT5)^+$ basal keratinocyte-like cells that self-organize into a cyst (Koehler et al., 2013), referred to hereafter as a skin organoid. In this article, we report that the mouse PSC-derived skin organoids recapitulate key steps of integumentary development and have the capacity to generate *de novo* HFs. Our results support an approach to generate skin and skin appendages from PSCs wherein the epidermal and the dermal cells are co-induced in a single organoid unit.

RESULTS

Modulating TGF, FGF, and BMP Signaling Pathways Initiates HF Formation in R1 mESC Aggregates

In our previous studies, we described a cell culture treatment regimen capable of inducing surface ectoderm in aggregates of mouse PSCs (Koehler et al., 2013; Koehler and Hashino, 2014). An initial treatment with a transforming growth factor β (TGF-β) inhibitor, SB431542 (SB), and recombinant BMP4 (BMP) specifies a surface ectoderm at the outermost region of the spheroid cell aggregates. A subsequent treatment with FGF-2 (FGF) and a BMP inhibitor, LDN-193189 (LDN), promotes induction of placodal epithelium. PAX8 is expressed in patches of the epithelium by day 8 (Koehler et al., 2013), suggesting induction of cells similar to those in a cranial region that produces epidermis as well as otic and epibranchial placode derivatives (e.g., the inner ear and sensory neurons in cranial nerves VII, VIII, and IX; Groves and Fekete, 2012). While the epithelium develops on the aggregate surface, PSCs persist in the aggregate core during the first week of differentiation (DeJonge et al., 2016). In addition, an intermediate tissue layer between the PSC core

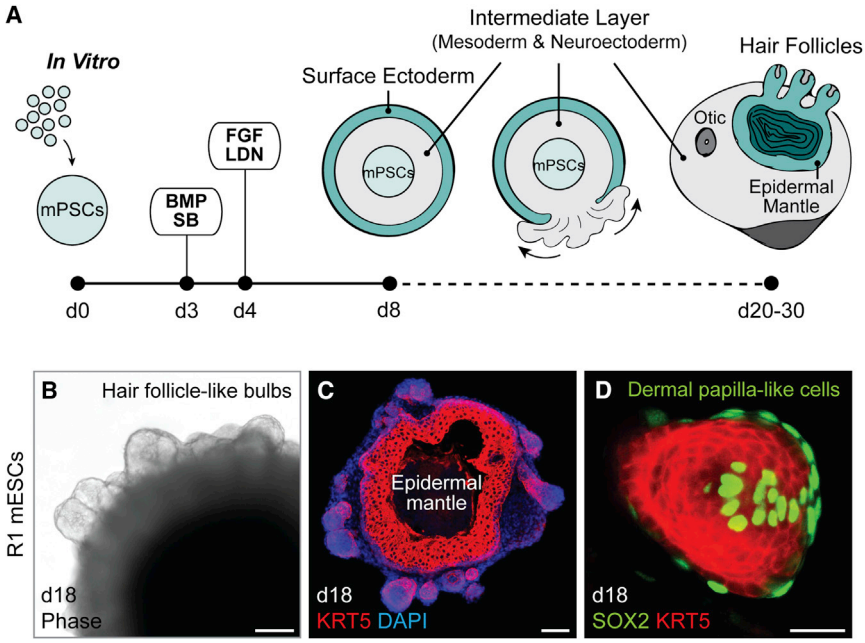

Figure 1. Spontaneous HF Bulb Development in R1 mESC Aggregates

(A) Schematic overview of mouse skin organoid culture. On day 0 of differentiation, dissociated mPSCs were cultured as an aggregate. On day 3, the aggregate was treated with SB and BMP to induce surface ectoderm, followed by day 4 treatment with FGF and LDN to induce placodal epithelium. By day 8, the aggregate comprises an undifferentiated PSC core, an intermediate layer containing mesoderm and neuroectoderm cells, and an outermost layer of surface ectoderm. From day 8, the aggregate is in a maturation medium and undergoes an inside-out transformation as the intermediate layer erupts out to cover the surface ectoderm.

(B) Representative phase contrast image. On day 18, bulb-like HFs protrude from the surface of an R1 mESC aggregate.

(C and D) Representative IHC images. HF-like bulbs with KRT5$^+$ epithelium in a skin organoid cryosection on day 18 (C) and a protruding KRT5$^+$ HF-like bulb structure with SOX2$^+$ DP-like cells (D). Scale bars represent 100 μm (B and C) and 50 μm (D). See also Figure S1.

and the surface ectoderm forms with Brachyury$^+$ mesendoderm cells and N-cadherin$^+$ SOX2$^+$ neuroectoderm cells (Koehler et al., 2013). During inner ear organoid production, otic vesicles evaginate from the epithelium, and the intermediate layer comprised of mesoderm/neuroectoderm cells erupts outward to form an outer layer, leaving the surface ectoderm inside as an epidermal mantle (inside-out morphology; Figure 1A). While investigating the otic culture system using the R1 mESC line, we observed the occasional formation of protruding bulb-like structures that differed in morphology from inner ear organoids (Figure 1B). We discovered that these structures were extensions of the KRT5$^+$ epidermis and were associated with SOX2$^+$ DP-like cells (Figures 1C and 1D), reminiscent of nascent guard, awl, or auchene HFs (Driskell et al., 2009; Lesko et al., 2013). This observation was made independently by the Koehler and Heller laboratory groups. In light of these unexpected findings, we sought to better characterize the process of folliculogenesis.

HF Formation Is Cell-Line and Aggregate-Morphology Dependent

The R1 cell line displayed relatively low frequency of HF production (18% ± 8% of aggregates with HF-like bulbs per batch, n = 84 organoids, 6 experiments; Table S1A). Surprisingly, while testing our otic induction method on other cell lines, we noted that an *Atoh1/nGFP* mESC line (Lumpkin et al., 2003; Oshima et al., 2010) was highly folliculogenic (Figure 2; Table S1A). As reported previously, this *Atoh1/nGFP* mESC line rarely produced inner ear organoids without an additional treatment with a GSK3β inhibitor, CHIR99021 (CHIR), on day 8 of differentiation (DeJonge et al., 2016). Without CHIR treatment, however, we found that *Atoh1/nGFP* cells produced a significantly higher percentage of HF-bearing aggregates than R1 aggregates (*Atoh1/nGFP*: 83% ± 5% of aggregates with HF-like bulbs per batch, n = 193 organoids, 10 experiments, $p < 0.0001$; Table S1A). To uncover differences between the cell lines, we examined the events leading to induction of skin organoids. Similar to the R1 cell line, we observed induced Brachyury$^+$ mesendodermal cells and ECAD$^+$ PAX8$^+$ epithelial cells during days 5–8 of differentiation of *Atoh1/nGFP* cells (Figure S1). By day 14, KRT5 was expressed in the epithelium in both R1 and *Atoh1/nGFP* organoids (n = 6 aggregates per cell line, 3 experiments; Figures 2A and 2B). Each aggregate typically contained a single skin organoid unit with KRT5 expressing cells forming a continuous spherical mantle-like structure (Figures 2A and 2B). While R1 cell aggregates appeared to have more pronounced growth of non-epithelial tissues around the KRT5$^+$ epithelium, such as neuroectoderm cells denoted by SOX2 expression (Figures 2A and S2A), most *Atoh1/nGFP* aggregates either lacked or had one patch of non-epithelial tissue attached to the skin organoid during days 12–18 (Figures 2B and S2A). Based on this observation, we classified day 18 *Atoh1/nGFP* aggregates into three categories to reflect the degree to which the epithelium was covered by exterior non-epithelial tissues: uncovered, partially covered, and fully covered (see Figure 2C, representative images). Moreover, we grouped HF-bearing organoids into three categories based on the number of HFs they produced: 1–5, 6–15, or >15 HFs (see Figure 2D, representative images). Aggregates in each category, which were sorted by the amount of exterior non-epithelial tissue, produced HFs (Figure 2E, center pie graph). However, uncovered or partially covered aggregates produced the highest percentage of skin organoids bearing >15 HFs, while fully covered *Atoh1/nGFP* aggregates, similar to R1 aggregates, rarely produced organoids with more than five HFs (Figure 2E, branched pie graph). Based on these observations, we questioned whether HF production is a unique predisposition of the R1 and *Atoh1/nGFP* cell lines. To answer this question, we cultured a C57BL/BJ induced PSC (iPSC) line using the same skin organoid induction protocol. The C57BL/BJ iPSCs

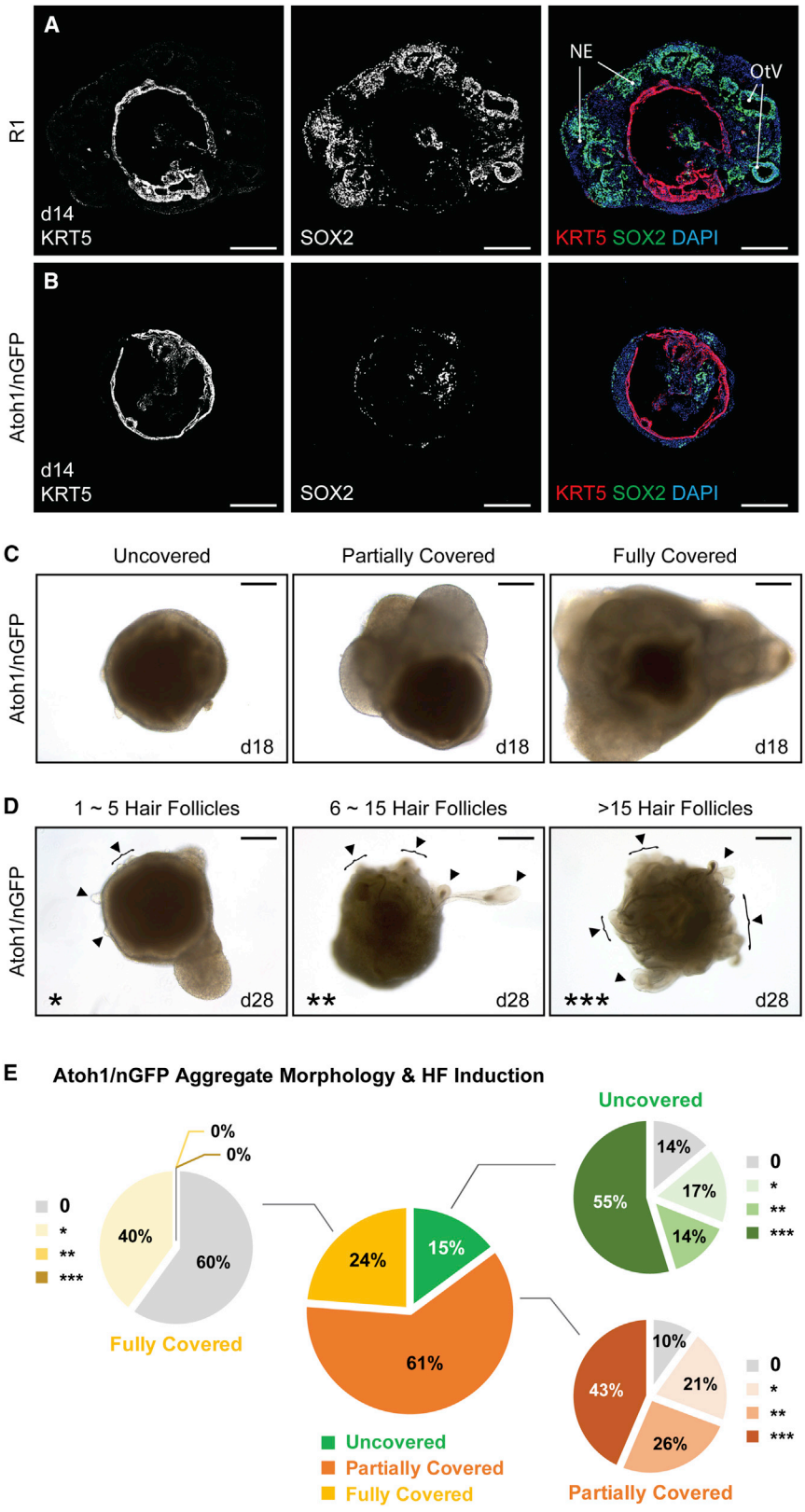

Figure 2. Comparison of R1 and *Atoh1/nGFP* mESC Developmental Morphologies and HF Formation

(A and B) Comparison of SOX2$^+$ neuroectoderm-like compartment and KRT5$^+$ epithelium formation between R1 (A) and *Atoh1/nGFP* (B) mESC aggregates during developmental stages, specifically on day 14. NE, neuroectoderm; OtV, otic vesicle.

(C) Representative DIC images of day 18 *Atoh1/nGFP* aggregates of each morphology category, based on the degree of the exterior tissues present outside the epithelium: uncovered, partially covered, and fully covered.

(D) Representative DIC images of day 28 *Atoh1/nGFP* aggregates of each HF-production category, based on the number of HFs produced: 1–5 HFs (*), 6–15 HFs (**), and >15 HFs (***). Arrowheads indicate HFs.

(E) The central pie graph represents percentages of *Atoh1/nGFP* aggregates in three different morphologies (uncovered, 29/193 aggregates; partially covered, 117/193 aggregates; and fully covered, 47/193 aggregates) categorized on day 18 of each experiment. The branched pie graphs represent percentages of aggregates categorized based on the production of HFs per morphology group, on days 22–31 (uncovered: 0, 4/29; *, 5/29; **, 4/29; ***, 16/29; partially covered: 0, 12/117; *, 24/117; **, 30/117; ***, 51/117; and fully covered: 0, 28/47; *, 19/47; **, 0/47; ***, 0/47 aggregates). Scale bars represent 200 μm (C and D) and 100 μm (A and B). See also Figure S2 and Table S1.

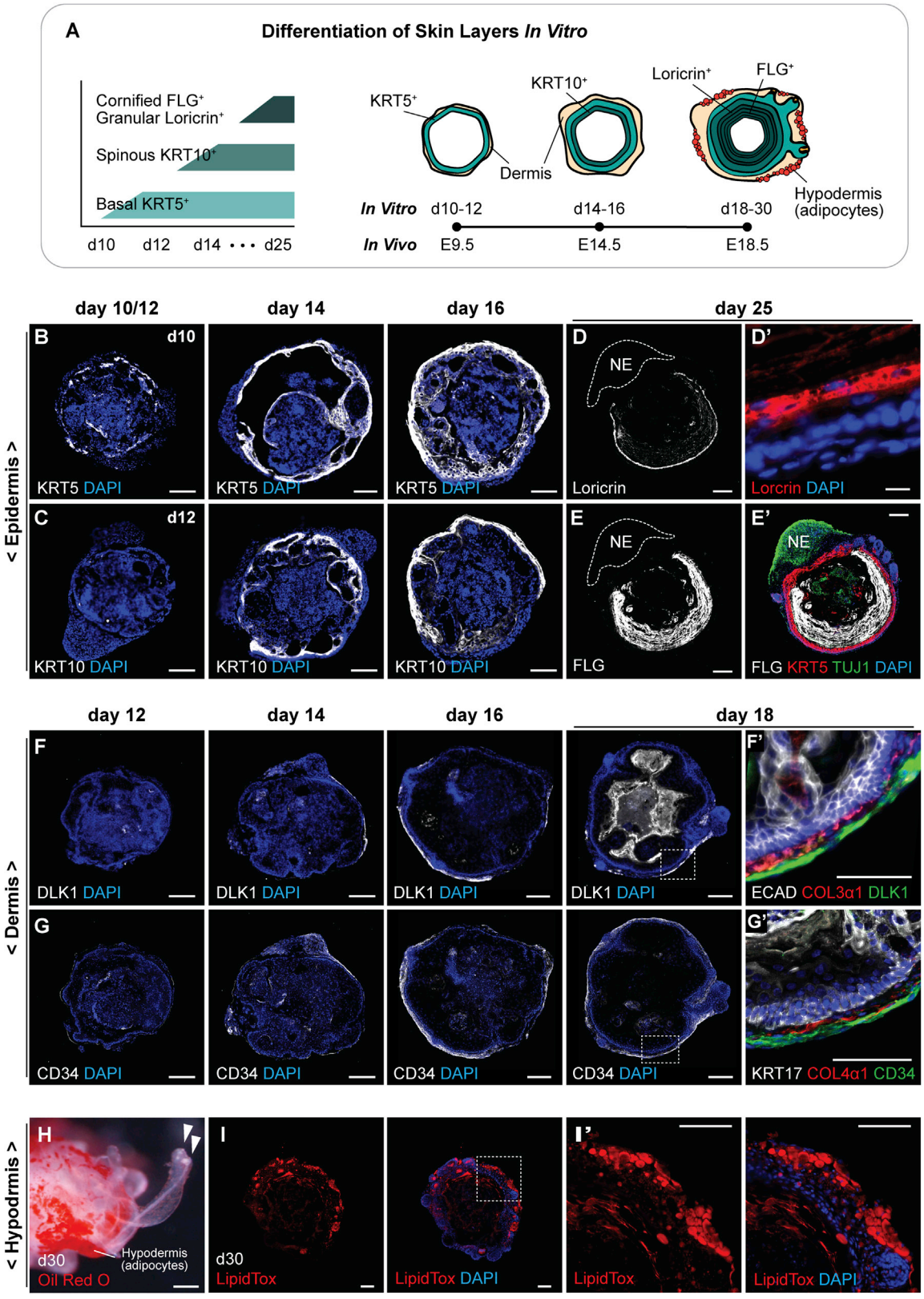

(legend on next page)

also generated HF-bearing skin organoids (Figure S2B), suggesting that robust induction of HF-producing skin organoids is not limited to one cell line. Moreover, as *Atoh1/nGFP* aggregates, uncovered or partially covered C57BL/BJ iPSC aggregates produced higher number of HFs compared to fully covered aggregates bearing only 0–2 HFs (data not shown). Together, these findings suggest that PSC line-specific characteristics affect the efficacy of HF production, whereas the general ability to produce HFs was observed in all three PSC lines.

Optimal Treatment Regimen for HF Induction

We next asked whether the complete SB, BMP, FGF, and LDN treatment regimen was necessary for HF induction. We knew from our previous work that SB/BMP-treated aggregates, without subsequent FGF and LDN treatment, produced epidermal keratinocyte cysts largely devoid of surrounding mesenchymal tissue (Koehler et al., 2013). Upon reexamination, we confirmed that HFs never developed when aggregates were grown in SB/BMP conditions (n = 12 aggregates, 3 experiments). Likewise, SB/BMP-FGF-treated aggregates produced epidermal cysts but were not folliculogenic (n = 12 aggregates, 3 experiments). Interestingly, SB/BMP-LDN-treated aggregates generated HF-bearing skin organoids, albeit inconsistently from batch to batch (46% ± 13% of organoids with HF-like bulbs per batch, n = 61 organoids, 8 experiments). However, we noted that the percentage of aggregates generating 15 or more HFs was significantly greater under the SB/BMP-FGF/LDN full-treatment condition compared to SB/BMP-LDN conditions (Table S1B; 45% ± 7% [SB/BMP-FGF/LDN] versus 13% ± 7% [SB/BMP-LDN] of organoids, respectively; $p < 0.01$). Thus, the full treatment of SB/BMP-FGF/LDN appears to be optimal for HF-bearing skin organoid formation. Moreover, when we treated the aggregates with CHIR on day 8, as used previously to encourage inner ear organoid induction (DeJonge et al., 2016), we found that presumptive HFs formed alongside inner ear organoids (Figure S2C). Consequently, the pulse of GSK3β inhibition does not disrupt HF induction.

Self-Assembly of Skin Organoids Recapitulates Embryonic Development

Using embryonic stem cell (ESC)- and iPSC-derived aggregates, we examined the integumentary developmental stages represented in our culture system (see schema in Figure 3A). In the developing murine skin, basal keratinocytes that express KRT5 are first observed in the surface epithelium at approximately embryonic day 9.5 (E9.5). Subsequently, intermediate or spinous keratinocytes that express KRT10 arise at ~E14.5. Finally, the granular and cornified epidermal layers that express loricrin and filaggrin (FLG) arise at ~E18.5 (Figure 3A). Remarkably, skin organoids develop stratified epidermis (Figures S3A and S3A′). We first observed KRT5 expression, indicative of basal keratinocytes, in patches of the ECAD$^+$ TFAP2α$^+$ epithelium on day 10 of differentiation (Figure 3B and S3B). We then noticed KRT10 expression in spinous-like epidermal cells by day 14 of differentiation (Figure 3C). Later, at day ~25, we observed robust expression of loricrin and FLG in granular and cornified layers of the organoid epidermis, respectively (Figures 3D-3E′ and S3B′). Interestingly, we noted that these mature epidermal markers were typically absent from sections of the epithelium abutting non-epithelial cells, such as TUJ1$^+$ neurons, suggesting that the composition of non-epithelial tissues may affect keratinocyte differentiation (Figures 3D–3E′ and S3B′).

Concurrently with epidermal layer development, a dermal layer was induced on the surface of skin organoids. In the developing mouse skin, the dermis stratifies to form three distinct collagen-rich layers during development. At ~E12.5, the dermis is composed of homogeneous dermal fibroblast progenitors, which later differentiates to form papillary and reticular dermal layers (E18.5), followed by an adipocyte-rich hypodermal layer (P2; Driskell et al., 2013). In our culture system, we noticed the presence of collagen type III, alpha-1 chain (COL3α1) and collagen type IV, alpha-1 chain (COL4α1) by day 12 of differentiation (Figure S3C); these are known extracellular matrix (ECM) proteins localized at the epidermal-dermal interface (Figures 3F′ and 3G′). The COL4α1 present on day 12 may be from Matrigel included in the medium on day 8; however, COL4α1 persisted throughout differentiation, suggesting that it may be produced endogenously (Figure 3G′ and S3C). Moreover, COL3α1, which is not a component of Matrigel, is also present at the epidermal-dermal interface beginning on day 12 and was present throughout differentiation (Figure 3F′ and S3C). By day 14 of differentiation, a dermal fibroblast-like cell marker, DLK1, was detected in cells around the epidermis (Figure 3F). As the skin organoids differentiate (from day 16), a DLK1$^+$ fibrotic region emerged in the dermal layer. Likewise, CD34, another fibroblast-like cell marker, was detected from day 12 surrounding the epidermis (Figure 3G). Interestingly, by day 16, CD34$^+$ cells were present throughout the dermal layer, while DLK1$^+$ cells were localized to discrete regions, suggesting that a diverse population of dermal cells may emerge in skin organoids (Figures 3F and 3G), consistent with late embryonic and early postnatal dermal development (Driskell et al., 2013). CD34 was expressed

Figure 3. Self-Assembly of Skin Layers in Skin Organoids

(A) Schematic overview of skin developmental stages *in vitro*. KRT5$^+$ basal keratinocytes are present on day 10, and KRT10$^+$ spinous-like epidermal cells are present by day 14. During days 18–30, a loricrin$^+$ granular layer and a FLG$^+$ cornified layer form. Developing HFs are visible by day 18. Dermis markers are observed on day 12 of differentiation and adipocyte-rich hypodermis forms by day 30.

(B–E′) Representative IHC images of self-assembled epidermis during days 10–25: KRT5$^+$ basal layer (B), KRT10$^+$ spinous layer (C), loricrin$^+$ granular layer (D and D′), and FLG$^+$ cornified layer (E and E′). (D, E, and E′) TUJ1$^+$ neuroectoderm cells are denoted NE.

(F–G′) Representative IHC images of dermis developed on days 12–18: DLK1$^+$ (F) and CD34$^+$ (G) dermal cells are formed surrounding the epidermis, and COL3α1 (F′) and COL4α1 (G′) are localized at the epidermal-dermal interface.

(H–I′) Representative hypodermis images. Adipocytes developed in the hypodermal layer are visualized by oil red O (H) and LipidTOX (I and I′) staining. Arrowheads (H) indicate two different protruding HFs.

Dashed-lined boxes (F, G, and I) indicate the area of magnification. Scale bars represent 100 μm (B–D and E–I′) and 10 μm (D′).

See also Figure S3.

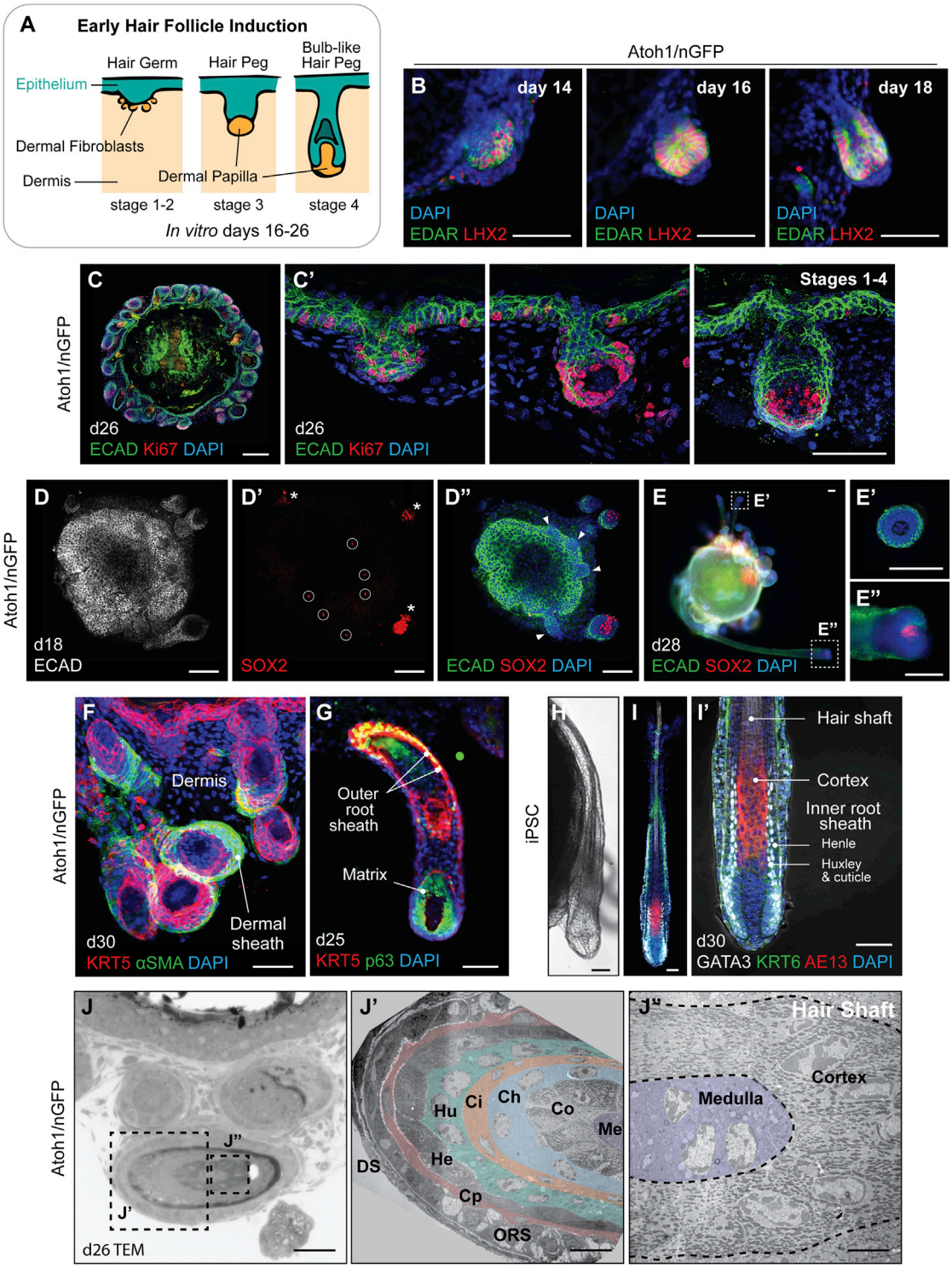

Figure 4. Stages of HF Induction Recapitulated in *Atoh1/nGFP* mESCs and miPSCs

(A) Illustration of the first four of eight stages of native HF development: hair germ, peg, and bulb formation.

(B) Representative IHC images of EDAR^{+} LHX2^{+} developing hair germs on days 14, 16, and 18.

(C and C′) Ki67^{+} cells in the hair germ and nascent HF matrix epithelium on day 26. Day 26 organoid contains HFs at different developmental stages (hair germs, pegs, and bulb-like hair pegs) in a single organoid unit.

(legend continued on next page)

in the dermal layer at later stages of differentiation as well (day 26; Figure S3C′). Pearl-shaped adipocytes started to appear on day 26 (Figures 3H–3I′), mimicking the maturation of fat in the hypodermis *in vivo*. Thus, the mouse skin organoids produced in our culture system recapitulate key features of skin differentiation on a timescale that roughly correlates with normal embryonic development.

Skin Organoid HF Induction Mimics Early Embryonic Developmental Stages

In mice, HF development has been classified into discrete stages (Paus et al., 1999; Figure 4A). During stage 1, at the site of HF induction, dermal papillary fibroblasts form a condensed mass as the epidermis thickens and protrudes to generate the hair germ. In stages 2–3, rapidly dividing Ki67$^+$ epithelial cells elongate the germ into a peg-like structure with DP cells at the terminal end. In stages 4–6, the hair pegs continue to elongate and thicken to form a bulb, cell layers of the inner and outer root sheaths become defined by morphology and expression of specific protein markers, and the hair cortex and shaft forms. In our *in vitro* system, hair germs were visible as early as days 14–18 of differentiation by double staining with EDAR and LHX2 (Figures 4B, S4A, and S4A′). Subsequently, HFs reminiscent of early-stage embryonic HFs (stages 1–4; Figure 4A) could be identified in skin organoids at any time point between differentiation days 18–26 (Figures 4C–4D″), suggesting that new HF induction is continuous during this time period. By day 18 of differentiation, all of the developing HFs contained SOX2$^+$ dermal condensates/DPs, indicating the development of nascent guard, awl, or auchene HFs (Figure 4D–4D″). Interestingly, however, at the later stage of differentiation by day 28, we also noticed the presence of HFs with SOX2-negative hair bulb region, reminiscent of zigzag HFs (Figures 4E-4E″, S4B, and S4B′). These findings suggest that skin organoids may be capable of producing at least two types of HFs—SOX2$^+$ guard, awl, or auchene HFs and SOX2$^-$ zigzag HFs—in a single skin organoid unit.

By dissecting the structural architecture of more mature-looking HFs after day 24 of differentiation, we discovered that the HFs generated within our skin organoids shared key features with HFs in embryonic stages 7–8. The HFs consisted of an outermost layer of αSMA$^+$ dermal sheath (Figure 4F), KRT5$^+$ p63$^+$ outer root sheath (Figure 4G), GATA3$^+$ inner root sheath layers (Figures 4H–4I′), Ki67$^+$ p63$^+$ HF matrix (Figure 4C, 4C′, and 4G), and AE13$^+$ cortex cells in the HF shaft (Figures 4I, 4I′, and S4D″). The proper organization of the HF in the skin organoid was revealed by transmission electron microscopy (TEM), showing all of the HF lineages formed from the outermost dermal sheath to the center of the hair shaft medulla (Figures 4J–4J″). Together, these findings reveal that skin organoids produced in our culture system can generate HFs similar to those seen in late embryonic and early postnatal development, consisting of all major units, including HF matrix, inner root, outer root, and dermal sheath layers.

Specialized Epidermal and Dermal Cellular Compartments Arise in Skin Organoids

In addition to the basic HF components outlined above, our skin organoids are composed of other epidermal and dermal microniches. During embryonic stages 7–8, neural-crest-derived melanocytes in the HF matrix pigment the hair shaft, sebaceous glands (SGs), and arrector pili muscles develop, and the dermis forms a hypodermal layer rich with adipocytes (Paus et al., 1999). We investigated whether these key cellular niches of the pilosebaceous unit arise in skin organoids (Figure 5A). For these analyses, we utilized both floating and Matrigel-embedding methods for organoid cultures. In the floating culture, the HFs typically wrapped tightly around the organoid (Figure 5B; Movie S1), whereas the HFs grew outward in Matrigel droplets, making it easier to assess HF morphology (Figure 5B′). We noted that not all organoid HFs had normal morphology; each organoid we examined contained at least one abnormal HF, which will require further analysis to define abnormal characteristics (Figure 5B′, arrowheads). Restricting analysis to HFs with normal morphology, we identified ITGα8$^+$ αSMA$^+$ muscle-like structures with elongated nuclei in the organoid dermis (Figures 5C and 5C′), which could indicate arrector pili muscle induction (Driskell et al., 2013). However, we did not observe elongated ITGα8$^+$ αSMA$^+$ cells with attachment points on the HFs and interfollicular epidermis as would be expected for fully formed arrector pili muscles. After 24 days of differentiation, we could detect SG-like structures on organoid HFs by oil red O and LipidTOX staining (Figures 5D–5D″). The structures were located near the HF attachment point with the epidermal mantle and co-expressed ECAD and SCD1, consistent with SG identity (Figures 5E, 5E′, and S4C–S4C″). The majority of SG-like structures observed in the skin organoids were bifurcates, reminiscence of guard hairs (Driskell et al., 2009). Moreover, as mentioned earlier in Figure 4D′, the SOX2$^+$ nuclei speckles in the skin epithelium were *Atoh1/nGFP*$^+$ ISL1$^+$ cells that arose in the epithelium between days 14 and 16 (Figures 5F–5F″), reminiscence of Merkel cells, which are touch-sensing cells in the epidermis (Lumpkin et al., 2003; Perdigoto et al., 2014). However, these cells were rarely

(D–D″) Day 18 skin organoid contains HFs with SOX2$^+$ DP (D′, *) and SOX2$^-$ germ stage HFs (D″, arrowheads). Sparse SOX2$^+$ interfollicular epithelial cells represent Merkel cells (D′, circles). See also Figures 5F–5F″.

(E–E″) On day 28, skin organoids have HFs containing or lacking SOX2$^+$ DP; HFs with SOX2$^-$ DP suggest a zigzag HF identity (E′), while HFs with SOX2$^+$ DP suggest guard, awl, or auchene HF identity (E″).

(F–I′) Representative images of developing HFs showing (F) αSMA$^+$ dermal sheath cells, (G) KRT5$^+$ p63$^+$ outer root sheath and p63$^+$ matrix cells. (H) Representative DIC image of an iPSC-derived HF on day 30. (I and I′) GATA3$^+$ inner root sheaths comprised of Huxley's and cuticle layers with Henle's layer, distinguishable by morphology. AE13$^+$ cells were located in the hair cortex region of organoid HF shafts.

(J–J″) TEM images of the *Atoh1/nGFP* ESC-derived skin organoid HF on day 26. (J′) Cross-section of the hair shaft showing HF lineages. From the outermost layer to the center of the HF: DS, dermal sheath; ORS, outer root sheath; Cp, companion layer; He, Henle's layer; Hu, Huxley's layer; Ci, inner root sheath cuticle; Ch, hair shaft cuticle; Co, cortex; Me, medulla. (J″) High-magnification view of the cortex and medulla.

Dashed-lined boxes (E and J) indicate the area of magnification. Scale bars represent 100 μm (B, C, and D–E″), 50 μm (C′, F–I′, and J), 10 μm (J′), and 5 μm (J″). See also Figure S4.

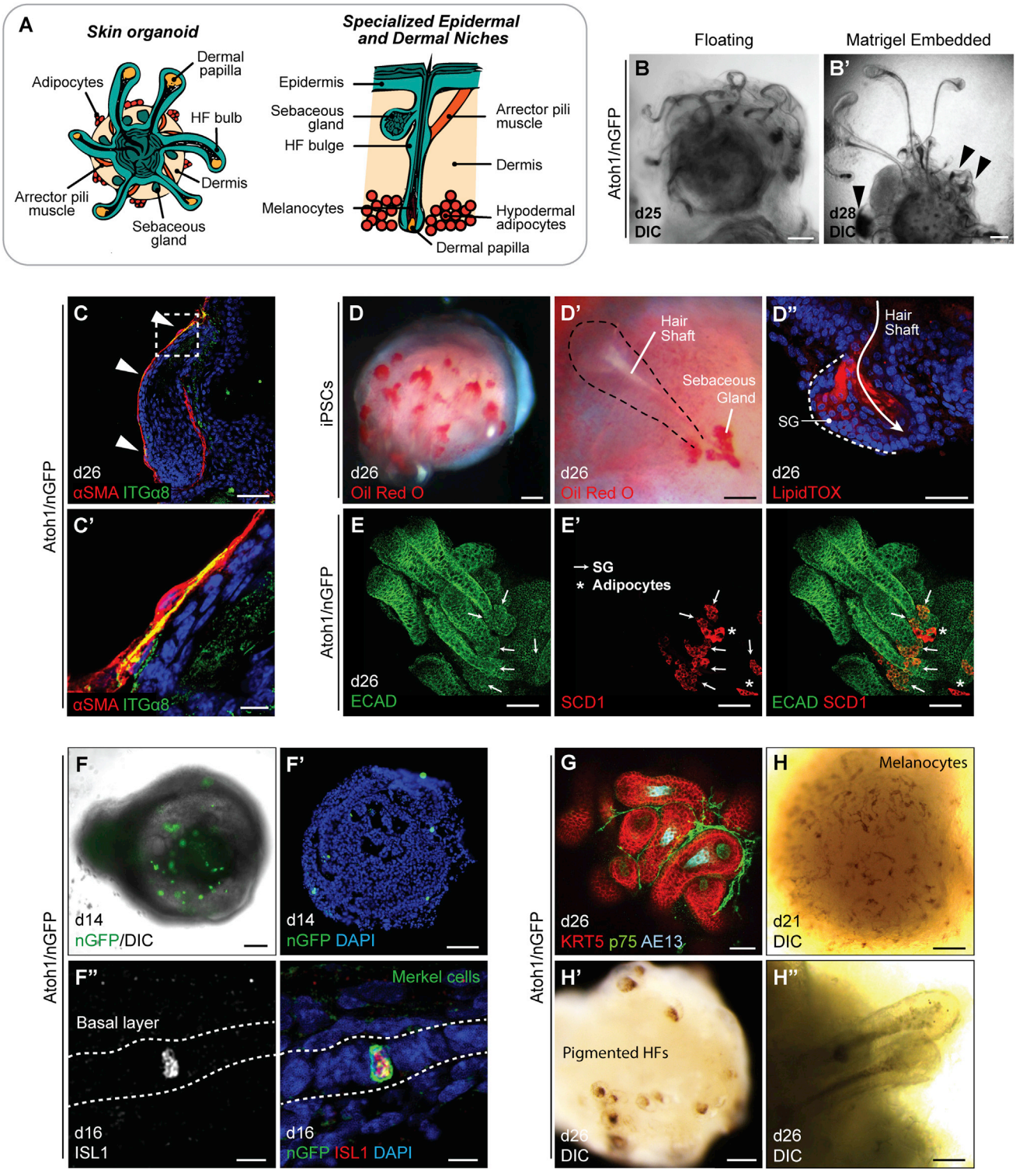

Figure 5. Specialized Cutaneous Cell Types in Skin Organoids

(A) Schematic of specialized epidermal and dermal niches within skin organoids. Late-stage (day >20) skin organoids consist of epidermis, dermis, and HFs (left). Close-up view of a single HF with sebaceous gland, arrector pili muscle, HF bulge, melanocytes in the hair shaft, and hypodermal adipocytes (right).

(B and B′) DIC images of HFs with entangled morphology in floating culture (B) and HFs with protruded morphology in Matrigel droplet (B′). Arrowheads denote abnormal HFs.

(legend continued on next page)

seen after day ~20 of differentiation (data not shown). We suspect that culture conditions or perhaps a lack of proper neuronal innervation may dysregulate Merkel cell development in the organoid culture format. Thus, further in-depth studies will be needed to additionally define our culture system for Merkel cell maturation.

Remarkably, we also observed p75$^+$ SOX10$^+$ neural-crest-like cells in the mesenchymal layer (Figures 5G and S4D–S4E′; Movie S1). In addition, melanocytes were visible around the epidermis as early as day 21 (Figure 5H) and migrated to and pigmented HFs in a subset of *Atoh1/nGFP* mESC-derived skin organoids by day 26 (Figures 5H′, 5H″, and S4F), suggesting that melanocytes can develop from the neural-crest-like cell population. However, melanocyte induction was infrequent during production of *Atoh1/nGFP* skin organoid production (12/252 organoids; other cell lines were not quantified). Together, our data suggest that the development of key skin and HF accessory tissues is recapitulated in skin organoids, but some cellular compartments (e.g., melanocytes) may depend on the composition of non-epithelial tissue associated with skin organoids.

Skin Organoid-Derived HFs Contain Bulge-like Regions

It has been reported that slow-cycling HF stem cells reside in a bulge region of the outer root sheath located proximal to the SG (Cotsarelis et al., 1990; Lavker et al., 2003). To determine whether organoid HFs develop a bulge-like region with the follicular stem cells, we adapted an EdU (5-ethynyl-2′-deoxyuridine)-labeling assay. As EdU incorporates into newly synthesized DNA, it makes possible to distinguish proliferating cell populations. In our culture system, we observed robust EdU incorporation in HF matrix cells (Figure 6A; Movie S2), which corresponded with Ki67$^+$ proliferating cells in the matrix (Figures 4C, C′, and 4G). EdU incorporation was less prevalent in regions of the HF above the matrix. Despite the sparse labeling, we consistently observed EdU incorporation in a subset of cells located in a bulge-like region near the SG in the upper outer root sheath (Figures 6A′ and 6A″; Movie S2). These cells may be hair follicle stem cell (HFSC)-like cells or SG progenitors. To further characterize cells in the bulge-like region, we examined known protein markers of HFSCs. We found that the HF bulge and epithelial stem cell markers, KRT15 and SOX9, were expressed broadly in the organoid HF outer root sheath as well as the bulge-like region (Morris et al., 2004; Nowak et al., 2008; Figures 6B–6B″). Nuclear-localized NFATc1 has been identified as a definitive marker of nascent and adult HFSCs, whereas CD34 is expressed in adult HFSCs of HFs that have entered the growth cycle (Horsley et al., 2008; Woo and Oro, 2011). We rarely observed KRT15$^+$ follicular cells that co-expressed CD34, indicating that organoid HFs likely do not contain adult HFSC-like cells (Figures 6B-B″and S4G–S4H′). By contrast, NFATc1 was specifically expressed by cells in the presumptive bulge region of organoid HFs between days 26 and 30 (Figures 6C and 6C′). Notably, NFATc1 expression was predominantly localized to the cytosol in bulge region cells; however, we observed nuclear-localized NFATc1 expression in the bulge regions of some HFs (n = 2 HFs from 9 organoids, ~40 HFs total; Figures 6C and C′). Based on previous studies, these data suggest that skin organoid HFs are capable of producing nascent HFSCs, reminiscent of HFSCs at a late embryonic (~E17.5) stage of development (Horsley et al., 2008). The rarity of cells expressing nuclear NFATc1 may indicate that the current culture conditions are not optimal for maturation of the bulge region stem cell niche.

Skin Organoid HFs Degenerate during Long-Term Culture

Finally, we examined whether skin organoid HFs undergo a catagen-like degenerative process similar to HFs *in vivo* as they enter the growth cycle. We tracked individual HFs over time using differential interference contrast (DIC) imaging (Figure 6D). We found that the HFs continued to grow until the experiment was terminated on day 32 while the growth rates gradually decreased day by day, and eventually, the HF matrix deteriorated around day 32, implying the possibility that the HFs undergo catagen (Figures 6D and 6E). To analyze whether the HFs truly undergo HF cycling in our culture system, we extended the culture period to 50 days and monitored HF growth (3 additional experiments). We did not observe newly forming HFs beyond days 32–35. Between 35 and 50 days, HFs appeared to have arrested growth and a dense layer of adipocytes forms on the surface of the organoids. We noted that skin organoid HF shafts cannot shed as they do *in vivo* during a typical HF growth cycle, which may lead to abnormalities in skin organoid HFs transitioning from development stages into the growth cycle. Partial dissociation and re-plating organoids in Matrigel droplets did not improve skin organoid longevity (data not shown). Thus, further studies will be necessary to explore ways of increasing the longevity of skin organoid cultures to potentially support *in vitro* HF cycling.

DISCUSSION

Our findings demonstrate that HF-bearing skin can be generated *in vitro* from a homogeneous source of mouse PSCs, under serum-free conditions. Not surprisingly, HF induction seems to be dependent on the co-development of both epidermal and dermal cells. In our culture system, the induction of epidermal cysts is highly reproducible across three PSC lines, yet the

(C and C′) αSMA$^+$ ITGα8$^+$ myocyte-like cells are occasionally observed in association with organoid HF dermal sheaths. Arrowheads denote αSMA and ITGα8 double-positive regions.
(D–E′) SGs near hair shafts were labeled by oil red O staining (D and D′), LipidTOX staining (D″), and whole-mount staining (E and E′). Arrows indicate SGs (SCD1$^+$ ECAD$^+$). Asterisks indicate adipocytes (SCD1$^+$ ECAD$^-$). SG; sebaceous gland.
(F–F″) Representative images of Merkel cells. DIC (F) and IHC (F′) images on day 14 show intermittent nGFP$^+$ cells, indicative of Merkel cells. nGFP$^+$ Merkel-like cells are also Islet1 (ISL1) positive (F″).
(G) A day 26 organoid with KRT5$^+$ HFs, p75$^+$ neural-crest-like cells, and AE13$^+$ HF cortex. p75 also labels dermal papilla cells.
(H–H″) Representative DIC images of melanocyte-like cells in the epidermis on day 21 (H) and pigmented HFs on day 26 (H′ and H″).
Dashed-lined box (C) indicates the area of magnification. Scale bars represent 250 μm (B′), 100 μm (B, E, E′, F, F′, H, and H′), 50 μm (C, D–D," G, H"), 10 μm (C', F"). See also Figure S4.

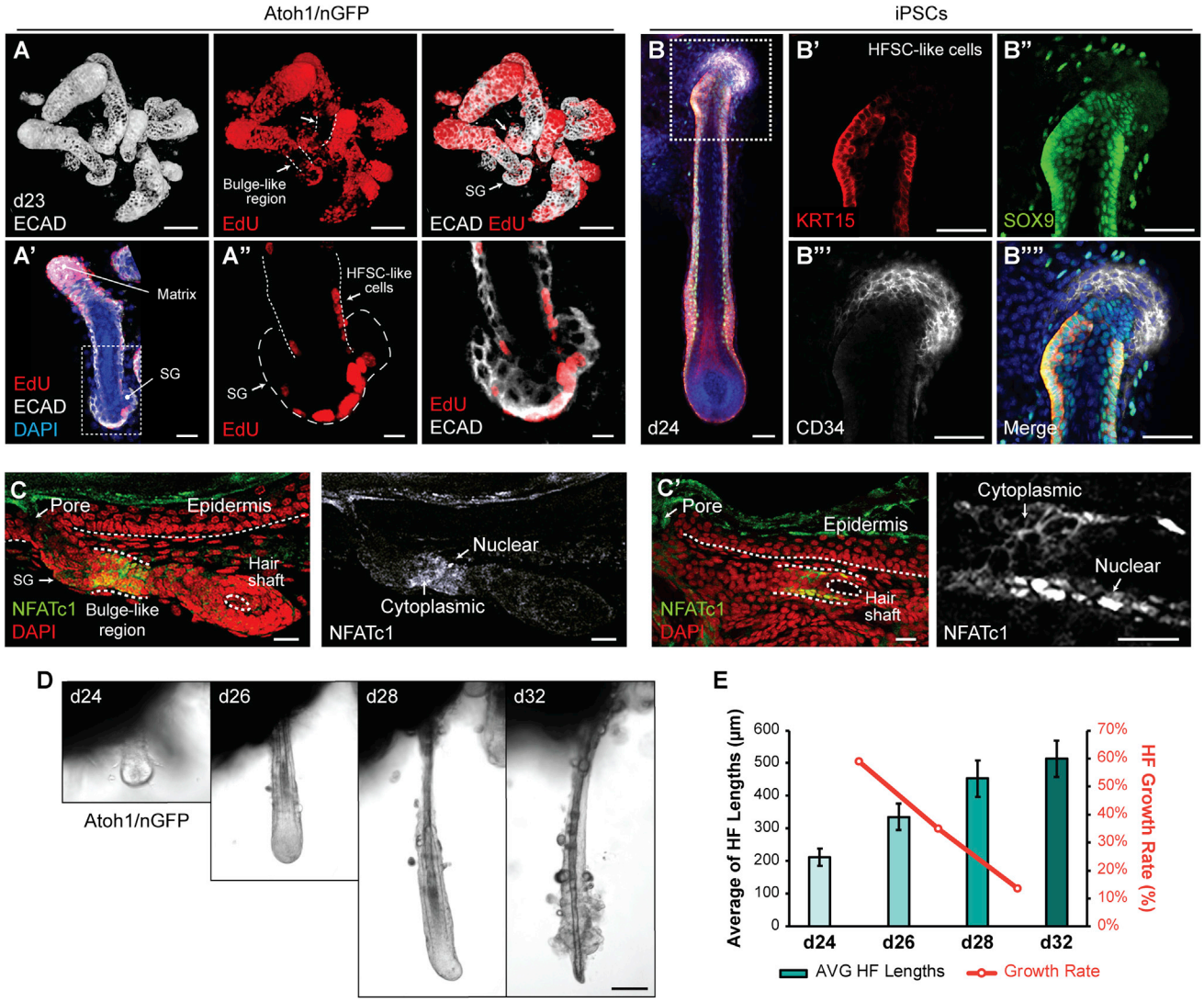

Figure 6. Development of HF Bulge-like Region and HF Degeneration in Skin Organoids

(A–A″) Representative day 23 images of HFs, which were incubated with EdU solution for 24 hr. EdU incorporation was noted in the HF matrix (A), outer root sheath, and SG (A′ and A″). Arrows indicate HF bulge-like region. SG, sebaceous gland; HFSC, hair follicle stem cell.

(B–B″″) KRT15^{+} SOX9^{+} CD34^{-} HFSC-like cells at early postnatal stage of maturity were present in the HF bulge-like region on day 24.

(C and C′) Representative IHC images of NFATc1 in the bulge-like region of two different *Atoh1/nGFP*-derived HFs. NFATc1 expression localized to the cytosol or nuclei of cells within the bulge-like region.

(D and E) HF morphologies were tracked during days 24–32 (D) after embedding aggregates in Matrigel on day 20 to fix aggregate position. Nine individual HFs were tracked to measure HF lengths, and HF growth rates were analyzed (E). HFs grew until day 32 while the growth rates of each interval were decreasing (D and E). HFs appeared to undergo degeneration starting on day 28 with protruding dermal papilla morphology; cells eventually lost integrity at the hair bulb region by day 32 (D).

Dashed-lined boxes (A′ and B) indicate the area of magnification. Bars denote ± SEM. Scale bars represent 100 μm (A and D), 50 μm (B–B″), 30 μm (A′, C, and C′), and 10 μm (A″). See also Figure S4.

frequency of accompanying induction of dermis and HFs appears to be cell-line dependent. Cell-line variability is a commonly cited shortcoming of organoid systems that rely on tissue self-assembly (Chen et al., 2014; Völkner et al., 2016). For our skin organoid system, the heterogeneity of the exterior tissue mass that forms during days 8–12 of differentiation likely underlies variability in HF induction. In particular, our data suggest that non-dermal tissues may be physically and/or chemically inhibitory to HF induction in floating aggregates. For example, R1 aggregates, which rarely generated HFs, contained a high abundance of neural tissue. By contrast, folliculogenic *Atoh1/nGFP* mESC and C57BL/BJ mouse induced pluripotent stem cell (miPSC) aggregates contained less non-dermal tissue. Thus, restricting the composition and self-assembly of the dermal layer to exclusively cutaneous cell types (e.g., fibroblast, adipocytes, and melanocytes) will be a challenge for future

studies on skin organoids. We found that minor modifications to the treatment concentrations and timing did not consistently improve or diminish the efficiency of HF induction. Thus, more targeted alterations must be made to gain control of dermis induction. One important consideration may be the use of physicochemically defined matrices, such as polyethylene glycol hydrogels, to replace Matrigel (Gjorevski et al., 2016).

To date, investigation into generating skin *in vitro* have focused on inducing pure populations of skin cell types (e.g. dermal fibroblasts or keratinocytes) from mouse and human PSCs (Coraux et al., 2003; Ehama et al., 2007; Guenou et al., 2009; Itoh et al., 2011, 2013; Mavilio et al., 2006). The logic of these approaches is that the individual parts can be combined to generate full-thickness skin (Itoh et al., 2013). This strategy, however, may lack the necessary crosstalk between cell layers to produce appendages that the current organoid approach preserves. Moreover, the organoid system may allow for induction of specific skin types (e.g., glabrous) with varying appendages. Based on our analysis, it is difficult to pinpoint the precise anatomical location represented by skin organoids; however, our data suggest that organoid derived skin may be similar to skin in the aural region—ear canal, auricular, or surrounding skin tissue. This hypothesis is supported by co-development of inner ear organoids and skin organoids, as well as expression of posterior surface epithelial and neuroepithelial marker PAX8 during differentiation (Ohyama et al., 2007).

Lastly, it is notable that the skin organoids assume a cyst conformation with radially oriented HFs. Seminal work in the 1940s and 1950s described the self-assembly of skin-organoid-like structures with protruding pigmented HFs (Hardy, 1949; Moscona and Moscona, 1952). In that work, epidermal and dermal cells from mouse embryos were excised, dissociated, and re-aggregated in a hanging drop of plasma. Likewise, HF-bearing cysts arise when dissociated embryonic skin from various mammals, including humans, is subcutaneously transplanted in mice (Zheng et al., 2005, 2010). More recently, a system for generating integumentary tissues was described in which mESC aggregates were partially differentiated and then placed in the kidney capsule of athymic mice (Takagi et al., 2016). Following transplantation, the aggregates preferentially differentiated into full-thickness skin layers in a cyst-like conformation and produced HFs. These results suggest that the derivation of multiple germ layers within a single stem cell aggregate may be a general strategy to produce hair-bearing skin. However, to date, this approach remains poorly defined and reliant on unknown microenvironmental factors within blood plasma or the subcutaneous and kidney capsule niches. Our study demonstrates how these skin organoid structures can be generated *de novo*, without the use of embryonic tissue or undefined media. We anticipate that this culture system will be useful for studying minimal cellular and microenvironment requirements for HF induction, evaluating HF growth/inhibitory drugs, or modeling skin diseases.

EXPERIMENTAL PROCEDURES

Generation of Induced PSCs

iPSCs (C57BL/BJ) were generated from C57BL/6 mouse embryonic fibroblasts (MEFs). See Supplemental Experimental Procedures for details.

PSC Maintenance Culture

ESCs (R1, kindly provided by Andras Nagy, and *Atoh1/nGFP*) and iPSCs (C57BL/BJ) were maintained in feeder-free conditions using LIF-2i medium as previously described (Koehler et al., 2013; Koehler and Hashino, 2014). See Supplemental Experimental Procedures for details and Table S2 for medium composition.

PSC Differentiation

Non-neural and placodal induction was performed as described previously, with modifications (Koehler et al., 2013; Koehler and Hashino, 2014). Differentiation on days 0–3 was slightly altered from what was described in the previous publications. Briefly, on day 0, PSCs were dissociated with 1X TrypLE Express Enzyme (GIBCO) or Accutase Cell Dissociation Reagent (GIBCO), re-suspended in ectodermal differentiation medium, and plated on 96-well low-cell-adhesion U-bottom plates (Nunclon Sphera, Thermo Scientific) at a final concentration of 3×10^3 cells per well in 100 μL. On day 1, 50 μL (half) of the spent medium in each well was removed and replenished with 50 μL fresh ectodermal differentiation medium containing 4% (v/v) Matrigel (final concentration of 2%; Corning). On day 3, 25 μL fresh ectodermal differentiation medium (without Matrigel) containing 50 ng/mL BMP-4 (PeproTech) and 5 μM SB431542 (Stemgent) was added to each well, which makes final concentrations of 10 ng/mL BMP-4 and 1 μM SB431542 in the final volume of 125 μL/well. For some experiments, the working concentration of BMP-4 was increased to final concentration of 50 ng/mL, which qualitatively improved skin organoid induction efficiency. On day 4, 25 μL fresh ectodermal differentiation medium (without Matrigel) containing 6 μM LDN (Stemgent) and 150 ng/mL FGF-2 (PeproTech) was added to each well, for final concentrations of 1 μM LDN and 25 ng/mL FGF-2 in the final volume of 150 μL per well. On day 8, each cell aggregate was transferred to individual wells on 24-well low-cell-adhesion plates (Nunclon Sphera) in 500 μL maturation medium containing 1% (v/v) Matrigel. Starting from day 10, half of the spent medium (250 μL) was removed and replenished with 250 μL fresh maturation medium (without Matrigel) every other day up to day 30. See Table S2 for media compositions.

Immunostaining

Frozen cryosections of aggregates prepared on slides and intact whole aggregates were used for immunohistochemistry (IHC) and whole-mount staining, respectively. Briefly, for IHC, the sections were blocked with 10% normal goat serum (NGS) or normal horse serum (NHS) (Vector Laboratories), incubated with primary and secondary antibodies diluted in 3% NGS or NHS, and mounted in ProLong Gold Antifade Reagent with DAPI (Molecular Probes). For whole-mount staining, the previously described Sca*l*eS protocol was adapted with major adjustments in incubation times to account for reduced tissue size (Hama et al., 2015). Briefly, the whole aggregates were adapted in Sca*l*e solution, permeabilized, descaled, immunostained, cleared, and mounted. Immunostained samples were visualized under Olympus FV1000-MPE or Leica TCS SP8 Confocal/Multiphoton microscopes. See Supplemental Experimental Procedures for details and Table S3 for a list of antibodies.

Oil Red O Staining

Oil red O staining was performed directly on the whole aggregate. The fixed and washed whole aggregate was placed in freshly prepared oil red O staining solution for 15 min at room temperature (RT). The solution was removed, and samples were washed with distilled water 5 times prior to imaging.

LipidTOX Staining

LipidTOX staining was applied on fixed and washed samples. Whole aggregates were incubated with LipidTOX neutral lipid stain diluted at a ratio of 1:200 in 1× PBS for 30 min at RT. The LipidTOX solution was removed and incubated in a Hoechst or DAPI solution for at least 30 min at RT to visualize nuclei. Samples were imaged using a wide-field upright microscope.

Fontana-Masson Staining

A Fontana-Mason staining kit (Abcam) was used to visualize melanocytes. The sections were incubated in ammoniacal silver solution until the sections turn into brownish color (~45 min), in 0.2% (v/v) gold chloride solution for 30 s,

and in 5% (v/v) sodium thiosulfate solution for 2 min, sequentially. Then, the samples were dehydrated in fresh absolute alcohol, cleared in Histochoice clearing agent (Sigma) for 2 min, and mounted in Organo/Limonene mount solution (Sigma). See Supplemental Experimental Procedures for details.

EdU-Labeling Assay

On day 22 of differentiation, a half volume of the spent medium was removed from the organoid culture, and an equal volume of fresh maturation medium containing 20 μM EdU solution was added, for a final EdU concentration of 10 μM. The organoids were incubated in 10 μM EdU containing medium for 24 hr, fixed in 4% paraformaldehyde (PFA) on day 23, immunostained for ECAD, cleared in Sca*l*eS4 solution, and imaged using a confocal microscope.

Image Analysis

Categorization of Aggregate Morphologies

The aggregates were categorized on day 18 into three different groups (uncovered, partially covered, and fully covered) based on the degree of exterior tissues around the epithelium. Sphere-like aggregates without tissue covering the epithelium were categorized into the uncovered group. Aggregates that still have a portion of exposed epithelium in the presence of a tissue mass located on one "pole" of the epithelial sphere are sorted as partially covered. When the epithelium was totally buried inside tissue, the aggregates were categorized into the fully covered group.

Determining the Number of HF-Bearing Aggregates

To determine the number of aggregates that have produced HFs, the aggregates that are on days 20–31, the time point when the HFs are very obviously presented, were counted and recorded. Organoids were rotated by shaking or with fine forceps for examination from multiple angles.

Categorization of HF-Bearing Aggregates

Aggregates containing HFs (days 20–31) were divided into 4 groups (0, *, **, and ***) based on the number of HFs present in each aggregate. If there was no HFs produced, the aggregate was categorized into 0 group. If 1 to fewer than 5 HFs were present, the aggregate was sorted into the * group. If 6 to fewer than 15 HFs were produced, the aggregate was categorized into the ** group. If more than15 HFs were formed, the aggregate was categorized into the *** group.

Measurement of HF Lengths

The lengths of individual HFs were tracked and measured from days 24 to 32. The aggregate was embedded in pure Matrigel on day 20, and DIC images of individual HFs were taken using a Leica DMi8 inverted microscope. Lengths of HFs were then measured using the Scale Bar tool in LAS X software. Because it is difficult to detect parts of HFs that are embedded in the center of the aggregate, the lengths were measured from the edge of the tissue mass, which had a dark outline, to the end of protruded hair bulge. The lengths of 9 individual HFs per aggregate were measured and averaged to calculate average HF length on days 24, 26, 28, and 32. The HF growth rate (%) from days 24 to 26, 26 to 28, and 28 to 32 were calculated using the following equation: (later day's HF length − earlier day's HF length)/earlier day's HF length × 100.

Statistical Analysis

All statistics were performed using GraphPad Prism 7 software. Statistical significance was determined using an unpaired Student's t test with Welch's correction to account for unequal SDs and sample sizes. Unless stated otherwise, data are reported as mean ± SEM. No statistical test was used to predetermine sample size, the investigators were not blinded to the treatment groups, and the samples were not randomized.

Representative Data and Reproducibility

Unless stated otherwise, images are representative of specimens obtained from at least 3 separate experiments. For IHC analysis of aggregates between days 0 and 8, we typically sectioned 3–6 aggregates from each condition in each experiment. IHC analyses for later stages of the protocol were performed on at least 3 aggregates from each condition per experiment. The culture method was replicated by five independent investigators (K.R.K., J.L., R.B., P.-C.T., and B.H.H.) using the cell lines listed above.

SUPPLEMENTAL INFORMATION

Supplemental Information includes Supplemental Experimental Procedures, four figures, three tables, and two movies and can be found with this article online at https://doi.org/10.1016/j.celrep.2017.12.007.

ACKNOWLEDGMENTS

The authors thank A. Mikosz, R. DeJonge, E. Longworth-Mills, and U. Arimpur for technical assistance and R. Nelson, E. Hashino, M. Rendl, and P. Rompolas for comments and resource sharing. We thank A. Nagy for the R1 ESCs. This investigation was conducted in a facility constructed with support from the NIH (grant C06 RR020128-01). This work was supported by the German Research Foundation (grant BO 4143/1-1 to R.B.), the NIDCD NRSA (grant DC013210 to B.H.H.), the Ralph W. and Grace M. Showalter Trust (K.R.K.), the Indiana CTSI (core pilot grant UL1 TR001108 to K.R.K.), the Indiana Center for Biomedical Innovation (technology enhancement grant to K.R.K.), and the NIH (grant DC006167 to S.H. and grant DC015624 to K.R.K.).

AUTHOR CONTRIBUTIONS

J.L., R.B., P.-C.T., B.H.H., and K.R.K. differentiated mPSCs; J.L., R.B., and K.R.K. performed analysis and interpretation of data; S.H. provided reagents and oversaw experiments; J.L. and K.R.K. conceived and designed experiments and drafted the manuscript with input from all authors; K.R.K. supervised and directed the study.

DECLARATION OF INTERESTS

J.L. and K.R.K, together with the Indiana University Research and Technology Corporation, have applied for a patent related to the cell culture method described in this manuscript. The remaining authors declare no competing interests.

Received: March 14, 2017
Revised: August 1, 2017
Accepted: December 4, 2017
Published: January 2, 2018

REFERENCES

Asakawa, K., Toyoshima, K.-E., Ishibashi, N., Tobe, H., Iwadate, A., Kanayama, T., Hasegawa, T., Nakao, K., Toki, H., Noguchi, S., et al. (2012). Hair organ regeneration via the bioengineered hair follicular unit transplantation. Sci. Rep. *2*, 424.

Chen, K.G., Mallon, B.S., McKay, R.D.G., and Robey, P.G. (2014). Human pluripotent stem cell culture: considerations for maintenance, expansion, and therapeutics. Cell Stem Cell *14*, 13–26.

Chuong, C.-M., Cotsarelis, G., and Stenn, K. (2007). Defining hair follicles in the age of stem cell bioengineering. J. Invest. Dermatol. *127*, 2098–2100.

Coraux, C., Hilmi, C., Rouleau, M., Spadafora, A., Hinnrasky, J., Ortonne, J.-P., Dani, C., and Aberdam, D. (2003). Reconstituted skin from murine embryonic stem cells. Curr. Biol. *13*, 849–853.

Cotsarelis, G., Sun, T.T., and Lavker, R.M. (1990). Label-retaining cells reside in the bulge area of pilosebaceous unit: implications for follicular stem cells, hair cycle, and skin carcinogenesis. Cell *61*, 1329–1337.

DeJonge, R.E., Liu, X.-P., Deig, C.R., Heller, S., Koehler, K.R., and Hashino, E. (2016). Modulation of Wnt signaling enhances inner ear organoid development in 3D culture. PLoS ONE *11*, e0162508.

Dequéant, M.-L., and Pourquié, O. (2008). Segmental patterning of the vertebrate embryonic axis. Nat. Rev. Genet. *9*, 370–382.

Driskell, R.R., and Watt, F.M. (2015). Understanding fibroblast heterogeneity in the skin. Trends Cell Biol. *25*, 92–99.

Driskell, R.R., Giangreco, A., Jensen, K.B., Mulder, K.W., and Watt, F.M. (2009). Sox2-positive dermal papilla cells specify hair follicle type in mammalian epidermis. Development *136*, 2815–2823.

Driskell, R.R., Lichtenberger, B.M., Hoste, E., Kretzschmar, K., Simons, B.D., Charalambous, M., Ferron, S.R., Herault, Y., Pavlovic, G., Ferguson-Smith, A.C., and Watt, F.M. (2013). Distinct fibroblast lineages determine dermal architecture in skin development and repair. Nature *504*, 277–281.

Ehama, R., Ishimatsu-Tsuji, Y., Iriyama, S., Ideta, R., Soma, T., Yano, K., Kawasaki, C., Suzuki, S., Shirakata, Y., Hashimoto, K., and Kishimoto, J. (2007). Hair follicle regeneration using grafted rodent and human cells. J. Invest. Dermatol. *127*, 2106–2115.

Fernandes, K.J.L., McKenzie, I.A., Mill, P., Smith, K.M., Akhavan, M., Barnabé-Heider, F., Biernaskie, J., Junek, A., Kobayashi, N.R., Toma, J.G., et al. (2004). A dermal niche for multipotent adult skin-derived precursor cells. Nat. Cell Biol. *6*, 1082–1093.

Gjorevski, N., Sachs, N., Manfrin, A., Giger, S., Bragina, M.E., Ordóñez-Morán, P., Clevers, H., and Lutolf, M.P. (2016). Designer matrices for intestinal stem cell and organoid culture. Nature *539*, 560–564.

Gledhill, K., Guo, Z., Umegaki-Arao, N., Higgins, C.A., Itoh, M., and Christiano, A.M. (2015). Melanin transfer in human 3D skin equivalents generated exclusively from induced pluripotent stem cells. PLoS ONE *10*, e0136713.

Groves, A.K., and Fekete, D.M. (2012). Shaping sound in space: the regulation of inner ear patterning. Development *139*, 245–257.

Guenou, H., Nissan, X., Larcher, F., Feteira, J., Lemaitre, G., Saidani, M., Del Rio, M., Barrault, C.C., Bernard, F.-X., Peschanski, M., et al. (2009). Human embryonic stem-cell derivatives for full reconstruction of the pluristratified epidermis: a preclinical study. Lancet *374*, 1745–1753.

Hama, H., Hioki, H., Namiki, K., Hoshida, T., Kurokawa, H., Ishidate, F., Kaneko, T., Akagi, T., Saito, T., Saido, T., and Miyawaki, A. (2015). ScaleS: an optical clearing palette for biological imaging. Nat. Neurosci. *18*, 1518–1529.

Hardy, M.H. (1949). The development of mouse hair in vitro with some observations on pigmentation. J. Anat. *83*, 364–384, 3 pl.

Horsley, V., Aliprantis, A.O., Polak, L., Glimcher, L.H., and Fuchs, E. (2008). NFATc1 balances quiescence and proliferation of skin stem cells. Cell *132*, 299–310.

Ikeda, E., Morita, R., Nakao, K., Ishida, K., Nakamura, T., Takano-Yamamoto, T., Ogawa, M., Mizuno, M., Kasugai, S., and Tsuji, T. (2009). Fully functional bioengineered tooth replacement as an organ replacement therapy. Proc. Natl. Acad. Sci. USA *106*, 13475–13480.

Itoh, M., Kiuru, M., Cairo, M.S., and Christiano, A.M. (2011). Generation of keratinocytes from normal and recessive dystrophic epidermolysis bullosa-induced pluripotent stem cells. Proc. Natl. Acad. Sci. USA *108*, 8797–8802.

Itoh, M., Umegaki-Arao, N., Guo, Z., Liu, L., Higgins, C.A., and Christiano, A.M. (2013). Generation of 3D skin equivalents fully reconstituted from human induced pluripotent stem cells (iPSCs). PLoS ONE *8*, e77673.

Koehler, K.R., and Hashino, E. (2014). 3D mouse embryonic stem cell culture for generating inner ear organoids. Nat. Protoc. *9*, 1229–1244.

Koehler, K.R., Mikosz, A.M., Molosh, A.I., Patel, D., and Hashino, E. (2013). Generation of inner ear sensory epithelia from pluripotent stem cells in 3D culture. Nature *500*, 217–221.

Lavker, R.M., Sun, T.-T., Oshima, H., Barrandon, Y., Akiyama, M., Ferraris, C., Chevalier, G., Favier, B., Jahoda, C.A.B., Dhouailly, D., et al. (2003). Hair follicle stem cells. J. Investig. Dermatol. Symp. Proc. *8*, 28–38.

Lesko, M.H., Driskell, R.R., Kretzschmar, K., Goldie, S.J., and Watt, F.M. (2013). Sox2 modulates the function of two distinct cell lineages in mouse skin. Dev. Biol. *382*, 15–26.

Lumpkin, E.A., Collisson, T., Parab, P., Omer-Abdalla, A., Haeberle, H., Chen, P., Doetzlhofer, A., White, P., Groves, A., Segil, N., and Johnson, J.E. (2003). Math1-driven GFP expression in the developing nervous system of transgenic mice. Gene Expr. Patterns *3*, 389–395.

Mavilio, F., Pellegrini, G., Ferrari, S., Di Nunzio, F., Di Iorio, E., Recchia, A., Maruggi, G., Ferrari, G., Provasi, E., Bonini, C., et al. (2006). Correction of junctional epidermolysis bullosa by transplantation of genetically modified epidermal stem cells. Nat. Med. *12*, 1397–1402.

Morris, R.J., Liu, Y., Marles, L., Yang, Z., Trempus, C., Li, S., Lin, J.S., Sawicki, J.A., and Cotsarelis, G. (2004). Capturing and profiling adult hair follicle stem cells. Nat. Biotechnol. *22*, 411–417.

Moscona, A., and Moscona, H. (1952). The dissociation and aggregation of cells from organ rudiments of the early chick embryo. J. Anat. *86*, 287–301.

Nakao, K., Morita, R., Saji, Y., Ishida, K., Tomita, Y., Ogawa, M., Saitoh, M., Tomooka, Y., and Tsuji, T. (2007). The development of a bioengineered organ germ method. Nat. Methods *4*, 227–230.

Nowak, J.A., Polak, L., Pasolli, H.A., and Fuchs, E. (2008). Hair follicle stem cells are specified and function in early skin morphogenesis. Cell Stem Cell *3*, 33–43.

Oh, J.W., Hsi, T.-C., Guerrero-Juarez, C.F., Ramos, R., and Plikus, M.V. (2013). Organotypic skin culture. J. Invest. Dermatol. *133*, 1–4.

Ohyama, T., Groves, A.K., and Martin, K. (2007). The first steps towards hearing: mechanisms of otic placode induction. Int. J. Dev. Biol. *51*, 463–472.

Oshima, K., Shin, K., Diensthuber, M., Peng, A.W., Ricci, A.J., and Heller, S. (2010). Mechanosensitive hair cell-like cells from embryonic and induced pluripotent stem cells. Cell *141*, 704–716.

Paus, R., Müller-Röver, S., Van Der Veen, C., Maurer, M., Eichmüller, S., Ling, G., Hofmann, U., Foitzik, K., Mecklenburg, L., and Handjiski, B. (1999). A comprehensive guide for the recognition and classification of distinct stages of hair follicle morphogenesis. J. Invest. Dermatol. *113*, 523–532.

Perdigoto, C.N., Bardot, E.S., Valdes, V.J., Santoriello, F.J., and Ezhkova, E. (2014). Embryonic maturation of epidermal Merkel cells is controlled by a redundant transcription factor network. Development *141*, 4690–4696.

Sun, B.K., Siprashvili, Z., and Khavari, P.A. (2014). Advances in skin grafting and treatment of cutaneous wounds. Science *346*, 941–945.

Takagi, R., Ishimaru, J., Sugawara, A., Toyoshima, K.-E., Ishida, K., Ogawa, M., Sakakibara, K., Asakawa, K., Kashiwakura, A., Oshima, M., et al. (2016). Bioengineering a 3D integumentary organ system from iPS cells using an in vivo transplantation model. Sci. Adv. *2*, e1500887–e1500887.

Toyoshima, K.-E., Asakawa, K., Ishibashi, N., Toki, H., Ogawa, M., Hasegawa, T., Irié, T., Tachikawa, T., Sato, A., Takeda, A., and Tsuji, T. (2012). Fully functional hair follicle regeneration through the rearrangement of stem cells and their niches. Nat. Commun. *3*, 784.

Völkner, M., Zschätzsch, M., Rostovskaya, M., Overall, R.W., Busskamp, V., Anastassiadis, K., and Karl, M.O. (2016). Retinal organoids from pluripotent stem cells efficiently recapitulate retinogenesis. Stem Cell Reports *6*, 525–538.

Woo, W.-M., and Oro, A.E. (2011). SnapShot: hair follicle stem cells. Cell *146*, 334–334.e2.

Zheng, Y., Du, X., Wang, W., Boucher, M., Parimoo, S., and Stenn, K. (2005). Organogenesis from dissociated cells: generation of mature cycling hair follicles from skin-derived cells. J. Invest. Dermatol. *124*, 867–876.

Zheng, Y., Nace, A., Chen, W., Watkins, K., Sergott, L., Homan, Y., Vandeberg, J.L., Breen, M., and Stenn, K. (2010). Mature hair follicles generated from dissociated cells: a universal mechanism of folliculoneogenesis. Dev. Dyn. *239*, 2619–2626.